

Two-dimensional energy transmitting boundary in the time domain

Naohiro Nakamura*

*Research & Development Institute, Takenaka Corporation, 1-5-1, Ohtsuka, Inzai, Chiba, 270-1395, Japan
(Received July 13, 2011, Revised September 8, 2011, Accepted October 30, 2011)*

Abstract. The energy-transmitting boundary, which is used in the well-known finite element method (FEM) program FLUSH, is quite efficient for the earthquake response analysis of buildings considering soil-structure interaction. However, it is applicable only in the frequency domain. The author proposed methods for transforming frequency dependent impedance into the time domain, and studied the time domain transform of the boundary. In this paper, first, the estimation methods for both the halfspace condition under the bottom of the soil model and the pseudo three-dimensional effect were studied with the time domain transmitting boundary. Next, response behavior when using the boundary was studied in detail using a practical soil and building model. The response accuracy was compared with those using viscous boundary, and the boundary that considers the excavation force. Through these studies, the accuracy and efficiency of the proposed time domain transmitting boundary were confirmed.

Keywords: energy transmitting boundary; FEM; time domain; soil-structure interaction; viscous boundary; excavation force

1. Introduction

The energy transmitting boundary (hereinafter referred to as “TB”), which is used in the programs FLUSH (Lysmer *et al.* 1975a) and ALUSH (Lysmer *et al.* 1975b) is a very precise and efficient wave boundary for lateral direction. These programs were developed in the 1970s and are still often used for structural studies in construction and civil engineering. TB was formulated in the frequency domain and therefore can only be used for linear analyses or equivalent linear analyses in the frequency domain (see Appendix A (1)). However, the availability of this boundary in terms of the time domain is also desired because buildings and the surrounding soil exhibit nonlinear behavior when a severe earthquake occurs.

Nakamura studied and proposed time domain transform methods for soil impedance that exhibits strong frequency dependency (Nakamura 2006a, b) and showed that these methods are very accurate. He also studied linear and nonlinear time history response analyses of a building considering the frequency dependent soil impedance (Nakamura 2008, 2009a). Then, TB for a two-dimensional (2D) in-plane problem that corresponds to FLUSH was transformed to the time domain, proving that it is possible to perform a highly accurate analysis in the time domain in a manner that is similar to that in the frequency domain (Nakamura 2009b) (see Appendix B). To

* Corresponding author, Ph.D., E-mail: nakamura.naohiro@takenaka.co.jp

prove the effectiveness of the transform method in solving nonlinear problems, he performed a response analysis using a building with nonlinear dynamic stiffness. However, these studies were limited to simple soil models.

In this paper, two additional functions of the time domain TB are studied, in order to expand the availability of the boundary. One is the semi-infinite condition at the bottom of soil models (hereinafter referred to as “the halfspace bottom condition”) in the calculation of TB. This function is necessary for many analyses considering the semi-infinite condition at the bottom of soil. The other function is the pseudo three-dimensional (3D) analysis with the anti-plane viscous damper. This function is also used to solve many problems in the frequency domain.

Next, the response analyses are conducted using a practical soil and building model to study the response characteristics more precisely. Soil maximum response values, soil impedance, and input motion, in addition to the building’s maximum response values are compared. Viscous boundary (Lysmer *et al.* 1969) (hereinafter referred to as “VB”), which is the most commonly used boundary for the response analysis in the time domain, is used for comparison, as was done in the previous study (Nakamura 2009b). In addition to the original VB model, a VB model considering the excavation force (hereinafter referred to as “VB + EF”) is studied. The excavation force (EF) is a correcting force of the boundary that is calculated in the TB formulation. It is known that the force increase the accuracy of the response result of VB. Thus, “VB + EF” is used in several analysis response programs, e.g. Super FLUSH (Kozo Keikaku Engineering Inc. *et al.* 2003). The formulation of VB and EF is shown in Appendix A (2).

2. Functional examination of the time domain TB

The previous paper indicates the study of a 2D in-plane problem with fixed conditions for the bottom of the soil model. In the analysis program using the frequency domain TB (such as Super-FLUSH), the following two functions are available. The first is the halfspace bottom condition, and the other is the pseudo 3D effect. These functions are considered useful even when the time domain TB is used. Next, the accuracy and efficiency of these functions are discussed in this chapter.

2.1 Functions for investigation

2.1.1 Halfspace bottom condition

Evaluation methods for the halfspace bottom condition in the calculation of time domain TB analysis is studied. The halfspace bottom condition for both the outer and inner fields is considered using VB. Although VB completely absorbs the wave projected from the direction perpendicular to the boundary surface, the accuracy decreases for waves projected from other directions. Since VB can be used for both time and frequency domains in the same manner, there are few problems concerning the outer and inner field models in the time domain. Therefore, the problem is related to the method and the accuracy when the halfspace bottom condition is applied for TB itself. The following two methods are considered for this purpose.

- (1) For calculating the TB matrix, VB could be integrated into the lowest layer during the stage of solving the eigenvalue problem related to the wave number. This method, proposed by Tajimi (1980) is used to calculate the point excitation solution of soil models using the thin layer element method (TLEM).

(2) A sufficient number of elements are added to the bottom of the soil model for the outer field used in the calculation of the TB matrix and the bottom of the added elements is considered to be fixed. The eigenmodes for only a part of the original soil model are used. The efficiency of the method for the frequency TB was studied by Okumura *et al.* (1982).

In this study, the second method is used for investigation.

2.1.2 Pseudo 3D effects

Although FLUSH is a program used for conducting 2D analyses, a method that considers approximate 3D effects by placing many viscous dampers in an anti-plane direction were proposed. This method is called the pseudo 3D analysis, and this boundary is called the anti-plane VB. Since this boundary can be used for both time and frequency domains in the same manner, few problems are related to the transform into the time domain. However, analysis accuracy needs to be verified in order for it to be used with the time domain TB.

2.2 Analysis models

The analysis model used in this study is shown in Fig. 1. The soil is two layered and the thickness of the surface layer is 40 m. The shear wave velocity (V_s) of the surface layer is 300 m/s and that of the bedrock is set for two cases. The first bedrock V_s is rigid and the next is 500 m/s. For the first case, a fixed bottom condition is used. For the second case, the characteristics of the bedrock are evaluated using the bottom VB in the inner and outer fields.

The building with a plane shape of $20\text{ m} \times 20\text{ m}$ is represented by the lumped mass model with shear spring elements. The height of the building is 24 m from ground level, and the depth of the basement is 10 m. The basement section is modeled by rigid elements. The causal hysteretic damping model (Nakamura 2007) is used for the building and the soil; the damping ratio is set to be 3% for the building and 2% for the soil. The physical properties of the soil and the building are shown in Tables 1 and 2, respectively. In the study, the distance from the outer edges of the building to the boundary (L) is set to either 5 m or 40 m.

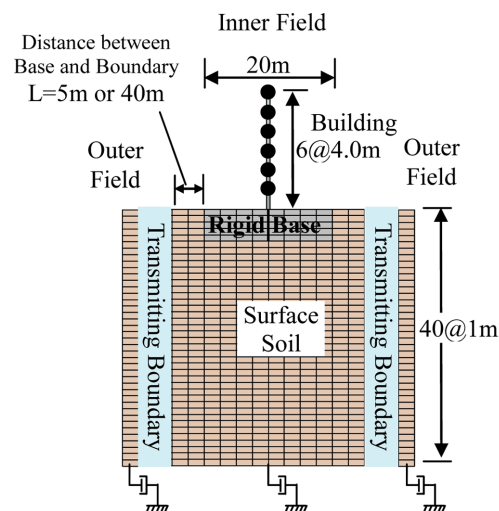


Fig. 1 Analysis model

Table 1 Property of soil

	Vs (m/s)	Poisson ratio ν	density ρ (t/m ³)	Damping ratio h	Thickness (m)
Surface	300	0.4	2.0	0.02	40
Bedrock	500	0.4	2.0	0	-

Table 2 Property of building

Story	Height (m)	Weight (t)	Rotational inertia (x10 ⁵ tm ²)	Shear stiffness (x10 ⁶ kN/m)
6	4.0	480	0	0.4935
5	4.0	480	0	0.9047
4	4.0	480	0	1.234
3	4.0	480	0	1.480
2	4.0	480	0	1.645
1	4.0	480	0	1.727
B1	5.0	720	1.2	∞

The analysis is conducted for a 2D in-plane problem with TB, and two cases - the frequency domain analysis using Super-FLUSH and the proposed time domain analysis - are compared. For the input motion, El Centro 1940NS wave (duration of 10 s, time step ΔT of 0.01s) with the maximum acceleration set to 500 Gal is used. For the fixed bottom boundary, the wave is inputted as E + F (sum of the upward wave and downward wave, equaling the motion at the position), and for the viscous bottom boundary, the wave is inputted as 2E (twice the upward wave). We used the Newmark- β method as a time integral method and an average acceleration method ($\beta = 1/4$).

2.3 Analysis results

To calculate TB matrix considering the halfspace bottom condition, a 100 m section of the elements having the bedrock properties is added to the bottom of the soil model. The maximum horizontal acceleration response of the above-ground part of the building obtained by the time domain analysis is compared to the results of the frequency domain analysis conducted using Super-FLUSH.

The responses in the case of the fixed bottom condition are shown in Table 3(a) for both $L = 5$ m and $L = 40$ m, and those in the case considering the halfspace bottom condition are shown in Table 3(b). The ratios of the time domain analysis results to the frequency domain analysis results range from 0.96 to 1.02 for Table 3(a), and from 0.96 to 1.01 for Table 3(b). It is also seen that there are few differences in the response for $L = 5$ m and $L = 40$ m in both tables.

The analysis indicates that the results for the time history response analysis considering the halfspace bottom condition correspond well with those for the frequency domain analysis, which is similar to the case of the fixed bottom condition.

Table 4 shows the maximum acceleration response for the above-ground part of the building when the pseudo 3D effect is considered. The anti-plane VB is added to the soil and the basement of the building in the inner field. The ratios of the time domain analysis results to the frequency domain analysis results range between 0.95 and 1.02 for the case of fixed bottom condition in Table 4(a),

Table 3 Comparison of maximum horizontal acceleration of building (m/s^2) on halfspace bottom condition

(a) Fixed bottom condition							(b) Halfspace bottom condition						
Height (m)	L = 5 m			L = 40 m			Height (m)	L = 5 m			L = 40 m		
	Freq. domain	Time domain		Freq. domain	Time domain			Freq. domain	Time domain		Freq. domain	Time domain	
24	158.0	157.6	1.00	158.0	156.8	0.99	24	38.64	38.24	0.99	38.14	37.51	0.98
20	143.6	141.4	0.99	143.6	140.9	0.98	20	29.12	29.29	1.01	29.02	28.71	0.99
16	121.4	122.0	1.01	121.4	121.4	1.00	16	22.46	22.54	1.00	22.44	22.09	0.98
12	97.65	99.38	1.02	97.64	98.90	1.01	12	18.64	18.32	0.98	18.54	17.88	0.96
8	71.47	72.46	1.01	71.47	72.20	1.01	8	14.23	13.71	0.96	13.73	13.37	0.97
4	44.08	43.62	0.99	44.09	43.62	0.99	4	8.48	8.24	0.97	8.44	8.16	0.97
0	26.05	24.99	0.96	26.04	24.94	0.96	0	6.57	6.32	0.96	6.52	6.30	0.97

Table 4 Comparison of maximum horizontal acceleration of building (m/s^2) on pseudo 3D effect

(a) Fixed bottom condition							(b) Halfspace bottom condition						
Height (m)	L = 5 m			L = 40 m			Height (m)	L = 5 m			L = 40 m		
	Freq. domain	Time domain		Freq. domain	Time domain			Freq. domain	Time domain		Freq. domain	Time domain	
24	165.9	164.6	0.99	175.7	174.3	0.99	24	37.59	37.19	0.99	38.38	37.76	0.98
20	146.5	139.5	0.95	151.7	144.5	0.95	20	28.59	28.93	1.01	29.49	29.60	1.00
16	123.3	121.7	0.99	126.9	124.9	0.98	16	22.41	22.73	1.01	23.26	23.34	1.00
12	99.04	99.12	1.00	101.7	101.3	1.00	12	18.72	18.79	1.00	19.61	19.56	1.00
8	71.64	71.71	1.00	73.35	73.08	1.00	8	13.66	13.51	0.99	14.05	13.94	0.99
4	42.85	41.64	0.97	43.80	42.51	0.97	4	8.66	8.80	1.02	9.00	9.08	1.01
0	25.88	26.31	1.02	26.46	26.78	1.01	0	6.60	6.50	0.98	6.71	6.60	0.98

and between 0.98 and 1.02 for the halfspace bottom condition (Table 4(b)). They indicate that the results of the time history response analysis correspond well with those of the frequency domain analysis when the anti-plane VB was added. In these cases, the responses between $L = 5$ m and $L = 40$ m are slightly different due to the effect of the anti-plane VB.

From the above results, it was verified that the halfspace bottom condition and the pseudo 3D effects can be evaluated with reasonable accuracy, even when the time domain TB is used.

3. Study using practical model

In the previous papers, the main objective was to explain the analysis method. Therefore the analysis models studied in the paper were relatively simple. In this chapter, the response analyses are conducted using a more realistic soil and building model to more precisely study the response characteristics and to confirm the efficiency and applicability of the method to more practical problems.

With regard to the response characteristics, we compared the soil's maximum response values, soil

impedance, and input motion, in addition to the building's maximum response values. For comparison, we used VB, which is the most commonly used boundary for the response analysis in the time domain. In addition to the original VB case, we also studied the VB + EF case (see Appendix A(2)).

3.1 Analysis models

The analysis model used in this study is shown in Fig. 2. The soil is multilayered with the shear velocity (V_s) ranging from 200 to 400 m/s on the top of the bedrock with V_s of 500 m/s. A height difference of 10 m is set at both ends of the soil. The characteristics of the bedrock are evaluated using the bottom VB.

The above-ground part of the building model is the same as that of the previous chapter. The height of the basement is set at 10 m. The physical properties of the soil are shown in Table 5. The damping model and the damping ratio for the building and the soil are also the same as that for the previous chapter. In this study, the distance from the outer edges of the building to the boundary (L) is varied within the range 5-100 m.

The analysis is conducted for a 2D in-plane problem and two cases (one with a time domain TB and another with a time domain VB) are compared. We also examined a case of EF + VB. The input ground motion and the time integral method are also the same as in the previous chapter.

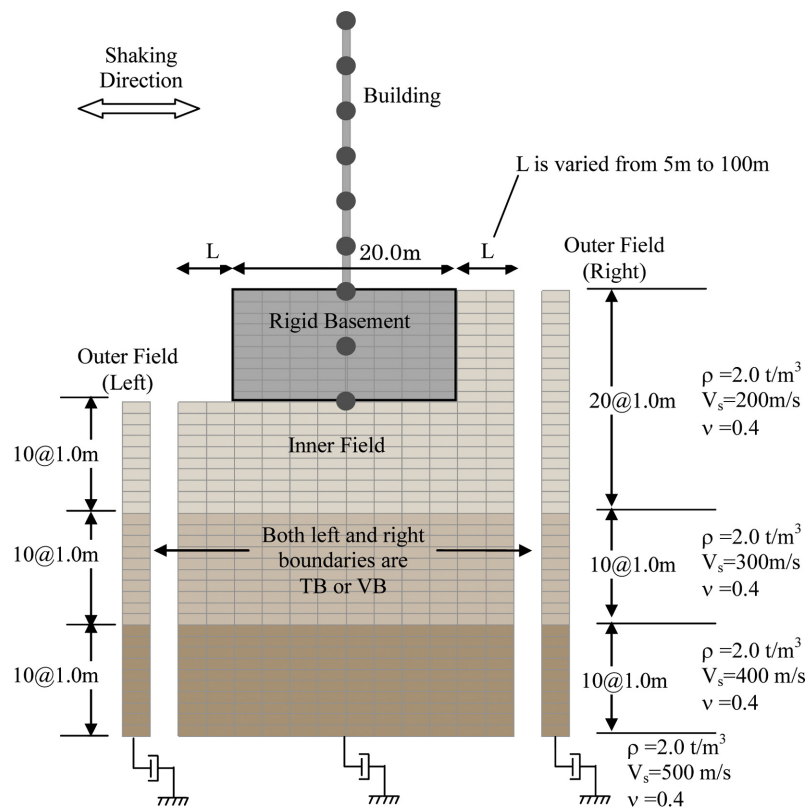


Fig. 2 More practical analysis model

Table 5 Property of soil

	Vs (m/s)	Poisson ratio ν	Density ρ (t/m ³)	Damping ratio h	Thickness (m)
Layer 1	200	0.4	2.0	0.02	20
Layer 2	300	0.4	2.0	0.02	10
Layer 3	400	0.4	2.0	0.02	10
Bedrock	500	0.4	2.0	0	-

Table 6 Property of building

Story	Height (m)	Weight (t)	Rotational inertia ($\times 10^5 \text{tm}^2$)	Shear stiffness ($\times 10^6 \text{kN/m}$)
R	-	480	0	-
6	4.0	480	0	0.4935
5	4.0	480	0	0.9047
4	4.0	480	0	1.234
3	4.0	480	0	1.480
2	4.0	480 <td 0	1.645	
1	4.0	720	0	1.727
B1	5.0	720	0	∞
B2	5.0	720	1.68	∞

3.2 Response of outer fields

Fig. 3 shows the distribution of the maximum response values for the outer fields (otherwise referred to as “free fields”) on the left and right sides. In this analysis, the displacement of the right side is larger. The maximum shear strain occurred at GL-20 m, which is the border between the layer with $V_s = 200$ m/s and that with $V_s = 300$ m/s, for both the left and right sides. The maximum strain on the right side is 0.32%, which is about twice the value on the left side.

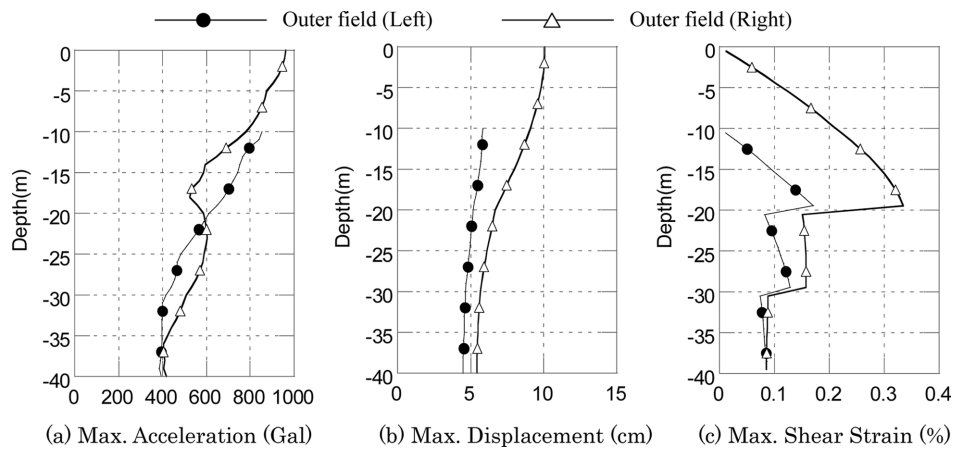


Fig. 3 Distribution of maximum responses of outer fields

3.3 Comparison of soil impedance

To investigate the validity of the proposed TB, the accuracy of the wave radiation is investigated by evaluating the soil impedance. To calculate the impedance of the foundation, the analysis model is created by deleting the building section from Fig. 2, and considering the basement to be a rigid structure with no mass. Both TB and VB are used for the side boundaries, and three cases for L (5, 40 and 100 m) are studied in the time domain.

An impulse force is applied at the center of the lower edge of the rigid basement in order to calculate the time history displacement of the basement. The time integral method was the same as that described in the previous section. The impulse force time history and the basement displacement time history are transformed by Fourier transform, and division in the frequency domain is performed to calculate the impedance. Three components of the impedance (horizontal, vertical and rotational) are studied. Although the coupling of the horizontal and rotational components is considered, only the diagonal components of the impedance matrix are investigated in this study.

The impedance of the rigid basement of the respective components is shown in Figs. 4-6. For comparison, the results of TB for L = 100 m are also shown in the figures showing the results of VB. The results of VB with L = 100 m and TB with L = 100 m agree well for all components. This indicates that the results for cases with L = 100 m are not significantly affected by the boundaries.

Fig. 4 shows the horizontal components of the impedance. TB, which is shown in Figs. 4(a) and (b), indicates a fairly large flutter with L = 5 m, but the total results with L = 5 m agree well with those with L = 100 m. Although there are slight differences below 3 Hz, comparisons between

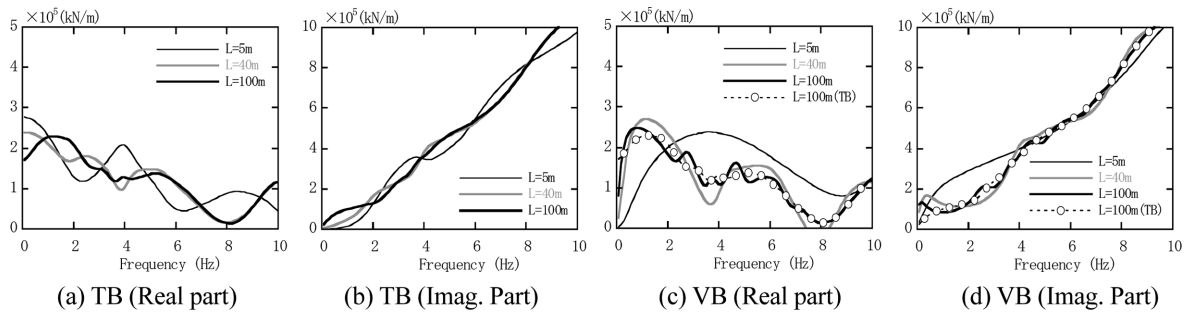


Fig. 4 Impedance of rigid foundation (Horizontal direction)

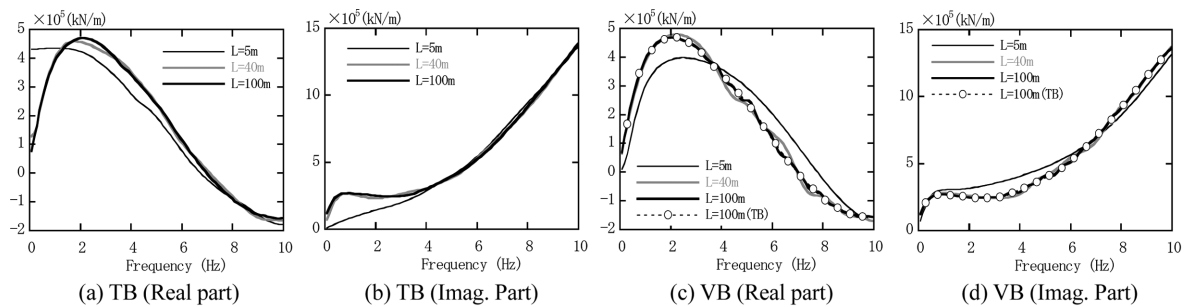


Fig. 5 Impedance of rigid foundation (Vertical direction)

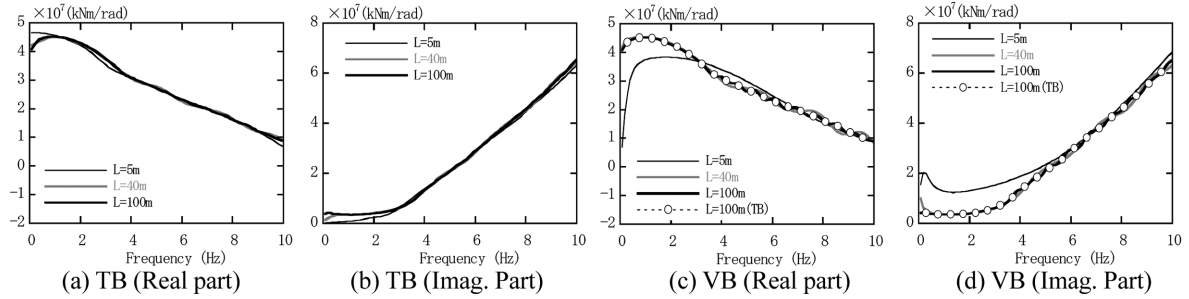


Fig. 6 Impedance of rigid foundation (Rotational direction)

$L = 40$ m and $L = 100$ m show that there is still better agreement than those between $L = 5$ m and $L = 100$ m. On the other hand, as shown in Figs. 4(c) and (d), with VB, there are large differences between the results for $L = 5$ m and $L = 100$ m. The case for $L = 40$ m corresponded to that of $L = 100$ m, however, the differences is larger than those in the case for $L = 40$ m and $L = 100$ m for TB.

Fig. 5 shows the vertical components of the impedance. Although there are some differences between the cases for $L = 5$ m and $L = 100$ m of TB and VB, the results for $L = 40$ m and $L = 100$ m corresponded favorably for this case. In all cases other than $L = 5$ m for TB, the real part tended to decrease rapidly near 0 Hz. This was considered to be due to the effect of the bottom boundary VB.

The trends are generally the same for the rotational components of the impedance, depicted in Fig. 6, all results except $L = 5$ m of VB, corresponded favorably for the results of $L = 100$ m of TB.

From above, for small values of L , such as $L = 5$ m, the impedance obtained using TB shows a relatively favorable accuracy, while that obtained using VB shows poor accuracy. On the other hand, both TB and VB offered a favorable accuracy for $L = 40$ m.

5. Comparison of input motion

Comparisons of the input motion are shown in Fig. 7. As described in the previous section, the building section is deleted except a rigid mass-less basement and an impulse wave is applied as the

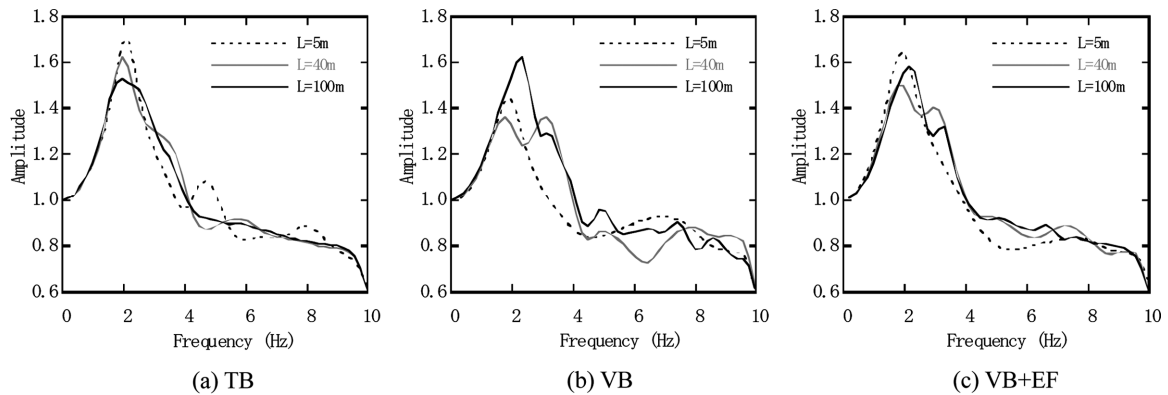


Fig. 7 Comparison of input motion

input ground motion from the bottom of the model as 2E. The acceleration response wave is calculated in the time domain at the centre of the bottom of the rigid basement. The acceleration response and the impulse input motion are transformed to frequency domain by Fourier transform, and divided to obtain the transfer function. This is evaluated as the input motion for the basement.

The case in which TB is used, depicted in Fig. 7(a), indicates a somewhat large flutter in the range of 4 to 8 Hz for $L = 5$ m. However, all cases ($L = 5, 40$ and 100 m) correspond favorably to the frequencies except the flutter with $L = 5$ m. In the case of VB, shown in Fig. 7(b), on the other hand, differences with $L = 100$ m exist for both $L = 5$ m and $L = 40$ m. Fig. 7(c) represents the cases of VB + EF. Accuracies for Fig. 7(c) are improved compared to Fig. 7(b) because results for both $L = 5$ m and $L = 40$ m approaches those of $L = 100$ m.

6. Comparison of responses for the soil near the building

The response values for the soil near the building are compared for all cases ($L = 5, 40$ and 100 m). In Fig. 8, the positions of this soil where response values are investigated are depicted with dotted lines. These lines are ranged from the ground surface to GL-40 m at the positions of one element (2.5 m) away from the left and right ends of the building.

The maximum response accelerations and displacements at both soil positions are shown in Fig. 9 for the cases for $L = 5$ m, 40 m and 100 m calculated using TB. The results for $L = 5$ m and $L = 40$ m corresponded well with those for $L = 100$ m. Table 7(a) indicates a range of ratios of the response values for $L = 100$ m at the soil positions. The gray section indicates that the maximum

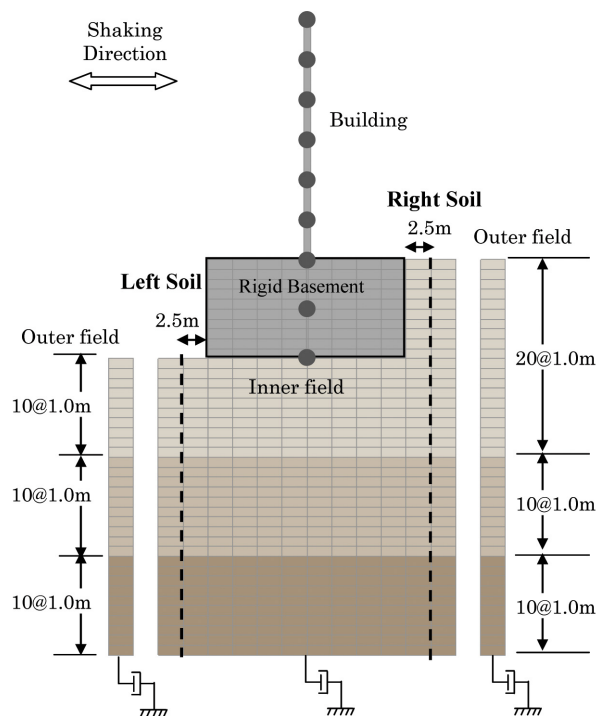


Fig. 8 Positions of soil where maximum responses are investigated

Table 7 Comparison of maximum responses of nearby soil

(a) TB		
Case	Acceleration	Displacement
L = 5 m	0.87 - 1.12	1.01 - 1.03
L = 40 m	0.97 - 1.05	1.00 - 1.01
(b) VB		
Case	Acceleration	Displacement
L = 5 m	0.80 - 1.17	0.83 - 1.13
L = 40 m	0.90 - 1.02	0.95 - 1.03
L = 100 m	0.97 - 1.03	0.99 - 1.01
(c) VB+EF		
Case	Acceleration	Displacement
L = 5 m	0.90 - 1.12	0.94 - 1.05
L = 40 m	0.96 - 1.03	1.00 - 1.01
L = 100 m	0.98 - 1.01	0.99 - 1.01

*(1) Values in these table show the range of maximum responses (Ratios to the response of TB, L = 100 m)

*(2) The color of each field shows the maximum difference (Black: more than 20%, Gray: between 10% to 20% and White: Less equal 10%)

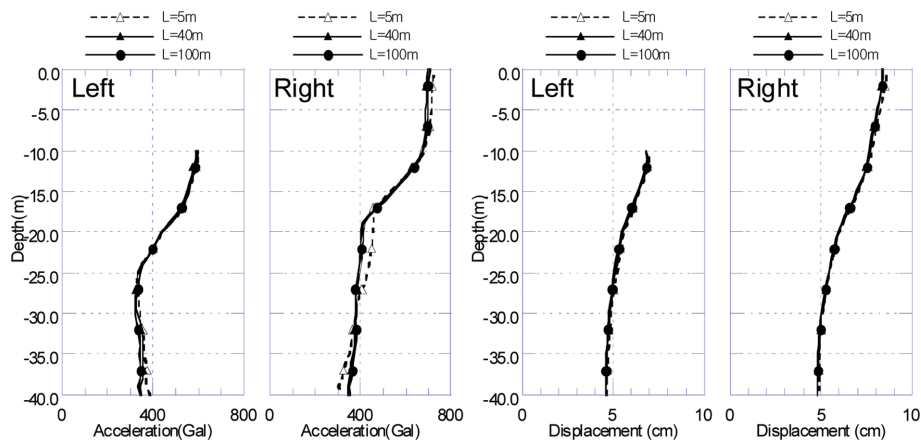


Fig. 9 Maximum responses of nearby soil (TB)

differences in the responses are 10% or more. In this case, the difference in the acceleration for L = 5 m was reached a maximum of 13%.

The maximum response values at both soil positions for the cases when VB are used are shown in Fig. 10. For comparison, this figure also shows the results of TB for L = 100 m. The results of L = 100 m of VB correspond well with those of L = 100 m of TB. There are, however, significant differences for L = 5 m with respect to L = 100 m and slight differences for L = 40 m with respect to L = 100 m. These differences are clearly larger than the case of TB, shown in Fig. 9. Table 7(b) indicates a range of ratios for the response values at both soil positions for L = 100 m using TB. The maximum difference is 20% for acceleration and 17% for displacement for L = 5 m.

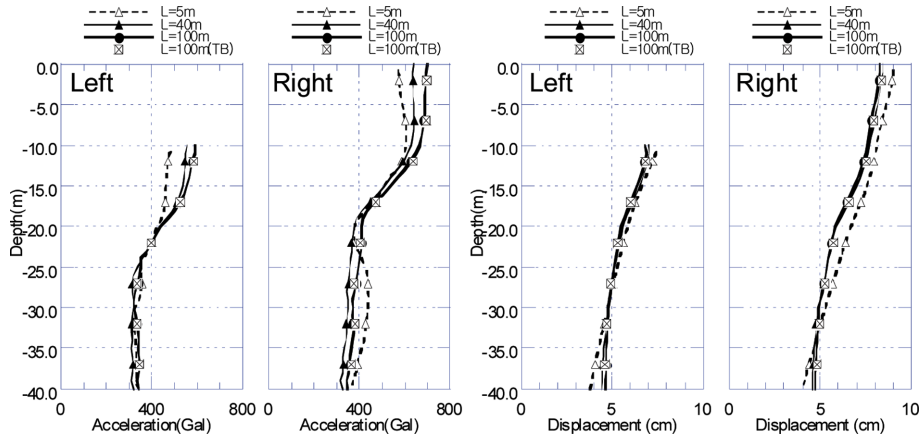


Fig. 10 Maximum responses of nearby soil (VB)

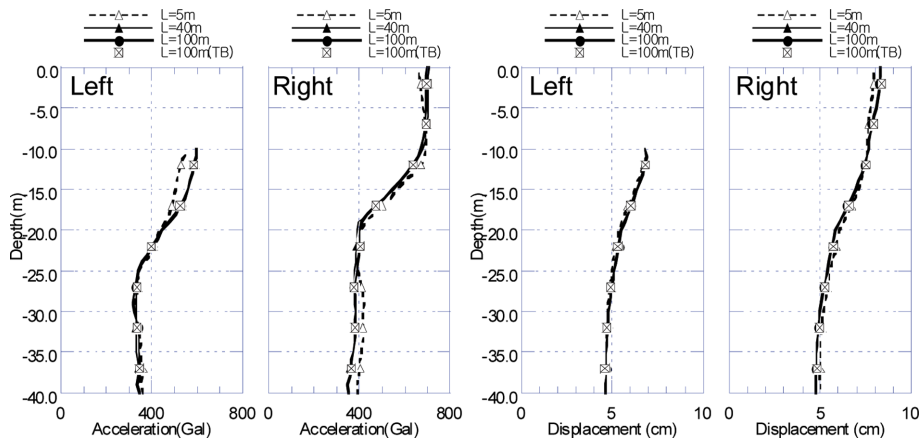


Fig. 11 Maximum responses of nearby soil (VB+EF)

The cases of VB + EF, as shown in Fig. 11, show improvements in accuracy in comparison with the case of VB shown in Fig. 10. Differences in acceleration for $L = 5$ m are up to a maximum of 12%, shown in Table 7(c), where the accuracy is the same as in the case of TB.

7. Comparison of response values for the building

Comparisons of the maximum response values for the above-ground part of the building are shown in Figs. 12-14. Fig. 12 shows maximum acceleration, maximum displacement and maximum shear force of the building for the case of TB. Although there are slight differences between the cases for $L = 5$ m and 100 m in terms of shear force, the total results of $L = 5$ m and 40 m correspond well with those of $L = 100$ m. The range of response ratios of $L = 5$ m and 40 m to $L = 100$ m at each building position are shown in Table 8(a). The differences in all components for both $L = 5$ m and $L = 40$ m are 7% or less.

The response values for the building when VB is used are shown in Fig. 13. For comparison, the

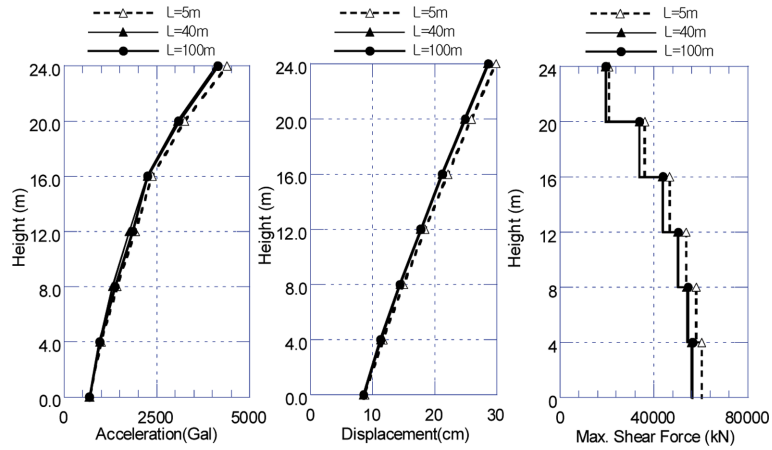


Fig. 12 Maximum responses of building (TB)

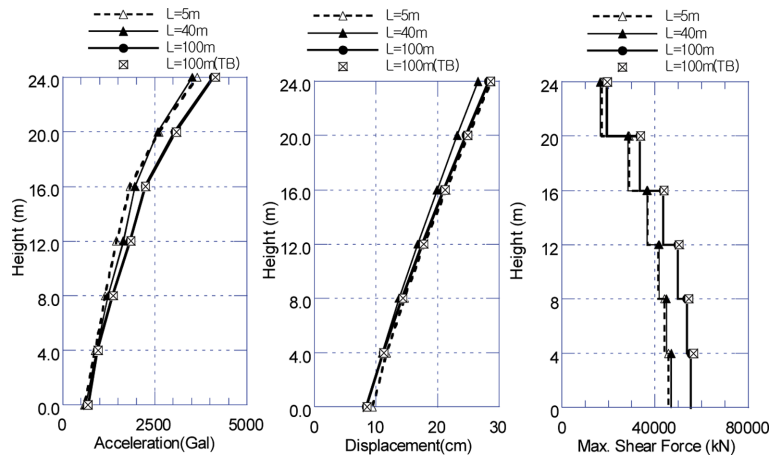


Fig. 13 Maximum responses of building (VB)

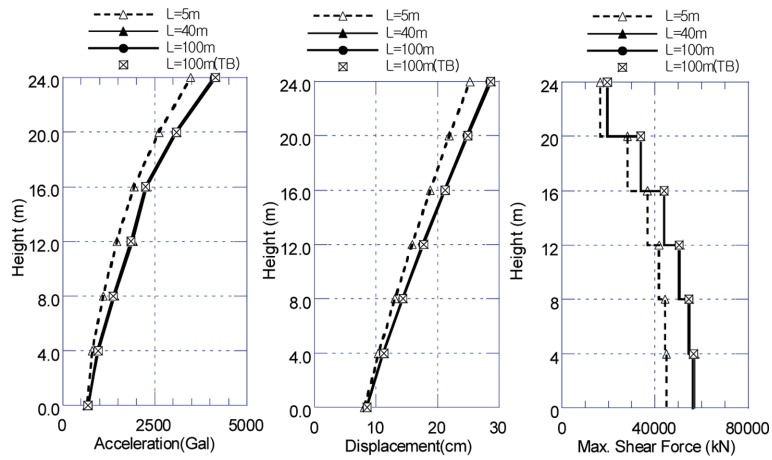


Fig. 14 Maximum responses of building (VB+EF)

Table 8 Comparison of maximum responses of building

(a) TB			
Case	Acceleration	Displacement	Case
L = 5 m	1.03 - 1.06	1.02 - 1.04	1.06 - 1.07
L = 40 m	0.95 - 1.00	0.99 - 1.00	0.99 - 0.99
(b) VB			
Case	Acceleration	Displacement	Case
L = 5 m	0.79 - 0.92	1.00 - 1.10	0.81 - 0.87
L = 40 m	0.84 - 0.97	0.93 - 1.00	0.83 - 0.83
L = 60 m	0.93 - 0.97	0.96 - 0.99	0.91 - 0.93
L = 80 m	0.97 - 0.98	0.98 - 0.99	0.97 - 0.98
L = 100 m	0.97 - 1.00	0.99 - 0.99	0.98 - 0.99
(c) VB+EF			
Case	Acceleration	Displacement	Case
L = 5 m	0.79 - 0.97	0.88 - 0.95	0.80 - 0.84
L = 40 m	1.00 - 1.03	1.00 - 1.00	1.00 - 1.01
L = 100 m	1.00 - 1.00	0.99 - 0.99	1.00 - 1.00

*(1) Values in these table show the range of maximum responses (Ratios to the response of TB, L = 100 m)

*(2) The color of each field shows the maximum difference (Black: more than 20%, Gray: between 10% to 20% and White: Less equal 10%)

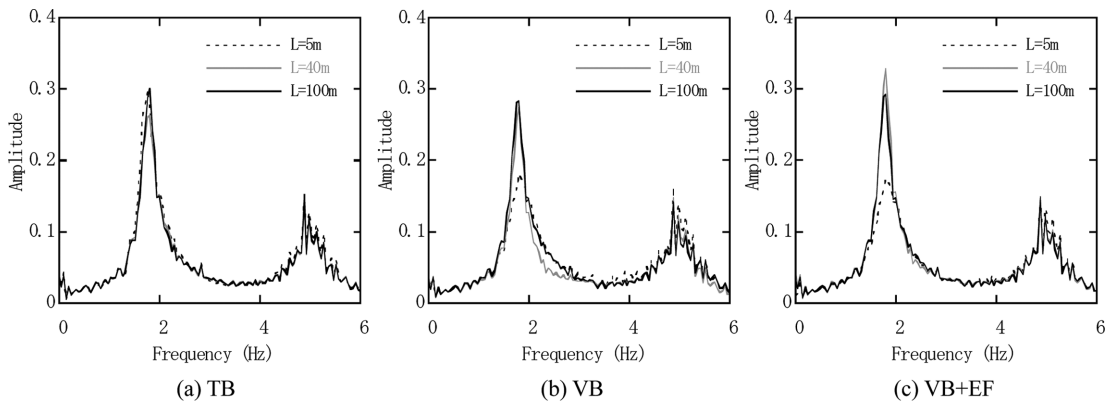


Fig. 15 Comparison of transfer functions

results of TB for L = 100 m are also shown in the figure. The figure shows that there are larger differences in the overall responses for the case of VB, in comparison to the case of TB. The differences in acceleration and shear force exceeded 10% for L = 40 m as well as 5 m. To reduce the differences to below 10% in this case, L = 60 m or more is needed.

Response values for the case VB + EF are shown in Fig. 14. The accuracy for L = 5 m does not differ much in comparison with the case when EF was not applied on VB, while the accuracy for L = 40 m improved.

Fig. 15 shows the transfer function of the response acceleration at the peak node of the building

Table 9 Accuracy of analysis results correspond to each boundary

(a) TB			
Case	Impedance	Input motion	Response
L = 5 m	Good	Good	Good
L = 40 m	Good	Good	Good
(b) VB			
Case	Impedance	Input motion	Response
L = 5 m	NG	NG	NG
L = 40 m	Good	NG	NG
(c) VB+EF			
Case	Impedance	Input motion	Response
L = 5 m	NG	Good	NG
L = 40 m	Good	Good	Good

for the input ground motion. The cases of using TB, shown in Fig. 15(a), indicate that the results of both $L = 5$ m and $L = 40$ m agreed very well with those of $L = 100$ m. In the case of VB, there is a large difference in terms of the peak height between $L = 5$ m and $L = 100$ m, as shown in Fig. 15(b). Although the peak height and positions corresponded to each other, there are differences of 2 or 3 Hz between the cases for $L = 40$ m and $L = 100$ m. For the cases of VB + EF, as shown in Fig. 15(c), the accuracy for $L = 40$ m improved, while the accuracy for $L = 5$ m remained low.

8. Summary of response

The outline of the analysis results is shown in Table 9. For VB, both the impedance and the input motion exhibited low accuracy when the L value was small. When the L value was increased to some extent, the accuracy of the response results did not increase since the accuracy of the input motion was low.

For VB + EF, the accuracy of the input motion improved and the response accuracy improved when the value of L was increased to a certain level. When the value of L was small, the response accuracy did not improve because of differences in impedance.

On the other hand, for TB, both the impedance and the input motion, as well as the response results, exhibited favorable accuracy for even small L values.

9. Conclusions

In this paper, the availability of two additional functions of the time domain TB was studied likewise in the frequency domain. One is the halfspace bottom condition in the calculation of TB. The other is the pseudo 3D effects using the anti-plane VB. It was verified that both functions can be evaluated with favorable degree of accuracy, when the time domain TB is used.

Next, in order to study the response characteristics more precisely, and to confirm the accuracy and efficiency of the method, a practical soil and building model was used. Then the impedance, input motion, soil maximum response values and building maximum response values were

compared to VB and VB + EF. From above, the effectiveness of the proposed time domain TB was confirmed.

References

- Kozo Keikaku Engineering Inc. and Jishin kougaku kenkyusho Inc. (2003), "Super FLUSH/2D theoretical manual Ver.4"
- Lysmer, J. and Kuhlelameyer, R.L. (1969), "Finite dynamic model for infinite area", *J. Eng. Mech.-ASCE*, **95**(EM3), 859-877.
- Lysmer, J., Udaka, T., Seed, H.B. and Hwang, R.N. (1975a), "FLUSH: a computer program for pseudo 3-D analysis of soil-structure interaction problems", Report No.EERC75-30, University of California, Berkeley.
- Lysmer, J., Udaka, T., Tsai, C.F. and Seed, H.B. (1975b), "ALUSH a computer program for seismic response analysis of axisymmetric soil-structure systems", Report No.EERC75-31, University of California, Berkeley.
- Nakamura, N. (2006a), "A practical method to transform frequency dependent impedance to time domain", *Earthq. Eng. Struct. D.*, **35**(2), 217-234.
- Nakamura, N. (2006b), "Improved methods to transform frequency dependent complex stiffness to time domain", *Earthq. Eng. Struct. D.*, **35**(8), 1037-1050.
- Nakamura, N. (2007), "Practical causal hysteretic damping", *Earth. Eng. Struct. D.*, **36**(5), 597-617.
- Nakamura, N. (2008), "Seismic response analysis of deeply embedded nuclear reactor buildings considering frequency dependent soil impedance in time domain", *Nucl. Eng. Des.*, **238**(7), 1845-1854.
- Nakamura, N. (2009a), "A Study on nonlinear seismic response analysis of buildings considering frequency dependent soil impedance in time domain", *Int. J. Int. Multis. Mech.*, **2**(1), 91-107.
- Nakamura, N. (2009b), "Nonlinear response analysis of soil-structure interaction system using transformed energy transmitting boundary in the time domain", *Soil Dyn. Earthq. Eng.*, **29**(5), 799-808.
- Okumura, M., Udaka, T., Tada, K. and Onami, M. (1982), "Efficiency of base viscous dashpot boundary on soil-structure interaction analysis", *Proceeding of 4th Symposium for computational system utilization*, Architectural Institute of Japan, 151-156.
- Tajimi, H. (1980), "A contribution to theoretical prediction of dynamic stiffness of surface foundations", *Proceeding of 7th World Conference on Earthquake Engineering*, Istanbul, Turkey, 105-112.

Appendix A: TB (Energy transmitting boundary) and VB (Viscous boundary)

1. TB

The formulation of the earthquake response analysis using a 2D in-plane TB in the frequency domain is briefly described below (Lysmer 1975a). The wave equation of the free field (outer field) in the 2-D in-plane problem is shown by Eq. (A1)

$$([A]k^2 + i[B]k + [G] - \omega^2[M])\{u^*(\omega)\} = \{0\} \quad (A1)$$

Here k : wave number, $\{u^*(\omega)\}$: displacement vector of the free field, and $[A],[B],[G],[M]$: matrices of $2n \times 2n$ (n : node number), which can be given as the superposition of the submatrices $[A]_j, [B]_j, [G]_j, [M]_j$ for each of the following elements.

$$\left. \begin{aligned} [A]_j &= \frac{h_j}{6} \begin{bmatrix} 2(2G_j + \lambda_j) & 0 & (2G_j + \lambda_j) & 0 \\ 0 & 2G_j & 0 & G_j \\ (2G_j + \lambda_j) & 0 & 2(2G_j + \lambda_j) & 0 \\ 0 & G_j & 0 & 2G_j \end{bmatrix}, [B]_j = \frac{1}{2} \begin{bmatrix} 0 & (G_j - \lambda_j) & 0 & (G_j + \lambda_j) \\ -(G_j - \lambda_j) & 0 & (G_j + \lambda_j) & 0 \\ 0 & -(G_j + \lambda_j) & 0 & -(G_j - \lambda_j) \\ -(G_j + \lambda_j) & 0 & (G_j - \lambda_j) & 0 \end{bmatrix} \\ [G]_j &= \frac{1}{h_j} \begin{bmatrix} G_j & 0 & -G_j & 0 \\ 0 & (2G_j + \lambda_j) & 0 & -(2G_j + \lambda_j) \\ -G_j & 0 & G_j & 0 \\ 0 & -(2G_j + \lambda_j) & 0 & (2G_j + \lambda_j) \end{bmatrix}, [M]_j = \frac{\rho_j h_j}{6} \begin{bmatrix} 2 & 0 & 1 & 0 \\ 0 & 2 & 0 & 1 \\ 1 & 0 & 2 & 0 \\ 0 & 1 & 0 & 2 \end{bmatrix} \end{aligned} \right\} \quad (A2)$$

Where, under the condition of Eq. (A3), the eigenvalue problem related to the wave number in Eq. (A4) is solved.

$$[C] = [G] - \omega^2[M] \quad (A3)$$

$$|[A]k^2 + i[B]k + [C]| = \{0\} \quad (A4)$$

From the obtained $4n$ eigenmodes, $2n$ modes corresponding to the waves propagating toward the right are extracted, and the mode matrix $[V]$ is set using these modes. $[K]$ is the diagonal matrix consisting of the eigenvalues. With this, the TB matrix of the model can be indicated by $[T_B]$ in Eq. (A5). $[D]$ is set with the superposition of the sub-matrix $[D]_j$. Although $[T_B]$ is not originally symmetric, in the following discussion, the matrix is made symmetric by averaging the terms at symmetric positions.

$$[T_B] = i \cdot [A][V][K][V]^{-1} + [D], \quad [D]_j = \frac{1}{2} \begin{bmatrix} 0 & \lambda_j & 0 & -\lambda_j \\ G_j & 0 & -G_j & 0 \\ 0 & \lambda_j & 0 & -\lambda_j \\ G_j & 0 & -G_j & 0 \end{bmatrix} \quad (A5)$$

Accordingly, the equation of motion for the entire model is given by Eq. (A6), where $[M_I]$: mass matrix of the inner field, $[K_I]$: stiffness matrix of the inner field and $\{u(\omega)\}$: displacement vector of the inner field.

$([T_B]-[D])\{u^*(\omega)\}$ indicates the boundary force vector in the case when seismic motion are being inputted from a vertical lower direction. In particular, $-[D]\{u^*(\omega)\}$ shows the additional force vector. This force is referred to as the excavation force.

$[T_B]$, $\{u^*(\omega)\}$ and $[D]$ are defined with $2n$ degrees of freedom in the boundary part up to Eq. (A5). However, hereafter they are extended to the number of degrees of freedom of the inner field to order to superimpose them on the values of the inner field.

$$(-\omega^2[M_I]+[K_I]+[T_B])\{u(\omega)\} = -\ddot{y}(\omega)[M_I]\{1\} + ([T_B]-[D])\{u^*(\omega)\} \quad (\text{A6})$$

2. VB

When VB is used, Eq. (A6) can be changed into Eq. (A7). $[V_B]$ is a diagonal matrix. V_{Bj} in Eq. (A8) is the j 'th diagonal component of $[V_B]$. Where, ρ : the density of the soil, V_S : shear velocity of the soil, V_P : primary wave velocity of the soil and A : corresponding section area (Lysmer *et al.* 1969).

$$(-\omega^2[M_I]+[K_I]+[V_B])\{u(\omega)\} = -\ddot{y}(\omega)[M_I]\{1\} + [V_B]\{u^*(\omega)\} \quad (\text{A7})$$

$$\left. \begin{array}{l} \text{For a horizontal degree or freedom: } V_{Bj} = \rho \cdot V_P \cdot A \\ \text{For a vertical degree or freedom: } V_{Bj} = \rho \cdot V_S \cdot A \end{array} \right) \quad (\text{A8})$$

When the excavation force is considered with VB, Eq. (A7) is changed into Eq. (A9) (Kozo Keikaku Engineering Inc. 2003).

$$(-\omega^2[M_I]+[K_I]+[V_B])\{u(\omega)\} = -\ddot{y}(\omega)[M_I]\{1\} + ([V_B]-[D])\{u^*(\omega)\} \quad (\text{A9})$$

Appendix B: Transform of $[T_B]$ matrix to time domain

Next, the transform of Eq. (A6) to the time domain is considered. The vectors $u(\omega)$, $\dot{u}(\omega)$ and $([T_B]-[D])\{u^*(\omega)\}$ can be transformed to the time domain using the usual inverse Fourier transform. Since the mass $[M_I]$ and stiffness matrices $[K_I]$ are not frequency dependent, no problems are encountered in the transform to the time domain. On the other hand, it is not easy to transform the frequency dependent matrix $[T_B]$ to the time domain. Therefore, the problem in the transforming Eq. (A6) to the time domain is reduced to transforming $[T_B]$ to the time domain. This section investigates this problem. First, the proposed transform methods are explained; then, the equation of motion in the time domain is described.

Although many methods to transform frequency dependent complex stiffness to the time domain have been proposed, most of them employed either the past displacement or the past velocity in the formulation of the impulse response. Nakamura (2006a, 2006b) proposed some transform methods using both the past displacement and velocity.

In this paper, following Method B' and Method C were used for the transform. The complex

stiffness and the reaction of method B' are expressed as shown in Eqs. (B1) and (B2), respectively.

$$S'_B(\omega) = -\omega^2 \cdot m_0 + i\omega \cdot c_0 + k_0 + \left\{ i\omega \cdot \sum_{j=1}^{n'} c_j \cdot e^{-i\omega t_j} + \sum_{j=1}^{n'} k_j \cdot e^{-i\omega t_j} \right\} \quad (\text{B1})$$

$$F'_B(t) = m_0 \cdot \ddot{u}(t) + c_0 \cdot \dot{u}(t) + k_0 \cdot u(t) + \left\{ \sum_{j=1}^{n'} c_j \cdot \dot{u}(t-t_j) + \sum_{j=1}^{n'} k_j \cdot u(t-t_j) \right\} \quad (\text{B2})$$

Where $u(t)$ is the displacement. $t_j = j\Delta t$ where Δt is the discrete time interval for the transform. It should be noted that Δt is usually different from ΔT (the time interval of the time history response analysis) as shown in Nakamura (2006a). c_j ($= c(t_j)$) and k_j ($= k(t_j)$) are the damping term and the stiffness term of the obtained impulse response function at t_j respectively. c_0 and k_0 are those of simultaneous components, while $c_{1 \sim n'}$ and $k_{1 \sim n'}$ are those of the time-delay components. m_0 is the simultaneous component of the mass term. All of the unknown impulse response components are solved by simultaneous equations with given complex stiffness data $D(\omega_i)$ ($i=0,1,2,\dots,N$).

In the case when the hysteretic damping is large, the accuracy of the recovered value of the complex stiffness tends to deteriorate. To improve this problem, the simultaneous components (m_0 , c_0 , k_0) are corrected. This method is called Method C'. The simultaneous components for the modified impulse response are set to be $m'_0 = m_0 + \Delta m$, $c'_0 = c_0 + \Delta c$ and $k'_0 = k_0 + \Delta k$. Where, Δm , Δc and Δk indicate the modification terms determined by the least square method (Nakamura 2008). The recovered value of the complex stiffness can be expressed using Eq. (B3).

$$S'_C(\omega) = S'_B(\omega) - \omega^2 \cdot \Delta m + i\omega \cdot \Delta c + \Delta k \quad (\text{B3})$$

Using Eq. (B3), the equation of motion in the frequency domain shown in Eq. (6) can be indicated in the time domain by Eq. (B4). Where $\{u(t)\}$ and $\{T^*(t)\}$ are values obtained using the inverse Fourier transform, which correspond to $\{u(\omega)\}$ and $([T_B]-[D])\{u^*(\omega)\}$, respectively.

The force $[T_B]\{u(\omega)\}$ in the frequency domain is separated into the simultaneous component $\{T_{B0}(t)\}$ and the time delay component $\{T_{B1}(t)\}$ in the time domain, as shown in Eqs. (B4) and (B5).

$$[M_I]\{\ddot{u}(t)\} + [K_I]\{u(t)\} + \{T_{B0}(t)\} = -\ddot{y}(t)[M_I]\{1\} + \{T^*(t)\} + \{T_{B1}(t)\} \quad (\text{B4})$$

Where

$$\{T_{B0}(t)\} = [m_0]\{\ddot{u}(t)\} + [c_0]\{\dot{u}(t)\} + [k_0]\{u(t)\}, \{T_{B1}(t)\} = -\sum_{j=1}^{n'} [c_j]\{\dot{u}(t-t_j)\} - \sum_{j=1}^{n'} [k_j]\{u(t-t_j)\} \quad (\text{B5})$$